Automatic operational modal analysis using statistical modelling of pole locations

S. S. Christensen [1], **A. Brandt** [1]
[1] Department of Technology and Innovation University of Southern Denmark,
Campusvej 55, 5230, Odense M, Denmark
e-mail: **ssv@iti.sdu.dk**

Abstract
Modal parameter extraction can be a time-consuming task. There are many applications where operator interaction is undesirable, for example for structural health monitoring. This paper presents an algorithm for automated operational modal analysis (AOMA) that utilizes one of the strong features of the stabilization diagram, namely the feature that physical modes tend to stabilize on the frequency axis for increasing model order. By employing statistical probability analysis and introducing a decision rule, that is based on the Modal Assurance Criteria (MAC), all modes in a user selected frequency range are automatically added to the output data-set. The algorithm has been tested on four different data-sets, a laboratory plexiglass plate, a suspension bridge, a medium-rise building and a ship. The results suggest that, the combined use of statistical probability analysis and a MAC based decision rule, successfully estimate modal parameters in an automated manner.

1 Introduction

Modal parameters can be estimated from response data using a modal parameter estimation (MPE) algorithm [1]. Regardless of what MPE that is chosen there will be a number of operator driven decisions to be made. With present day technology, that allows for more and cheaper sensors as well as faster computers, it is sought to automate such decisions, as they are the bottle necks when it comes to estimating modal parameters. This must be done in a fast and consistent way.

Recently, many attempts to build an automated operational modal analysis (AOMA) algorithm involve the use of clustering algorithms [2, 3, 4, 5]. Among clustering algorithms, the K-Means Clustering and the Agglomerative Hierarchical Clustering, are methods used for OMA. They both work in a multidimensional space and look to find the optimal clusters in a data-set through iteration. The K-Means Clustering requires a predefined number of clusters, while the Agglomerative Hierarchical Clustering does not, but instead combines clusters one by one until it is terminated by a stopping rule, or to the point where only a single cluster remains. Due to the way that clustering algorithms work, there are a few challenges, namely how to formulate the multidimensional space. In its simple form it includes frequency and damping, but can be extended to also include information about mode shapes, RMS levels etc. Furthermore, the K-Means Clustering is dependent on a predefined number of clusters, while the Agglomerative Hierarchical Clustering requires a trigger level that terminates the algorithm before it adds too many clusters together.

Another attempt to develop an AOMA algorithm would include histogram analysis [6]. This approach fits a probability distribution (a histogram) to the stabilization diagram to aid in selecting a vertical column. The stabilization diagram, a plot showing the number of poles (model order) as a function of frequency, is a strong tool to locate physical poles, since they tend to stabilize on the frequency axis for increasing model order. In this paper, we investigate this idea, and extend it by adding a few decision rules, in an attempt to construct an AOMA algorithm that is robust.

Section 2 briefly uncovers the fundamental theory to MPE, alongside the methodology of the proposed AOMA algorithm. In section 3, we show how the proposed AOMA algorithm is performing on various data-sets, namely a laboratory plexiglass plate, a suspension bridge, a medium-rise building and a ship. The concluding remarks are found in Section 4.

2 Theory

A stochastic process $x(t)$ passing through a linear time-invariant system, the output $y(t)$, also a stochastic process, is only dependent on the impulse response function (time domain), see Equation 1.

$$y(t) = h(t) * x(t) \tag{1}$$

The $*$ denotes the convolution operator. Equation 1 can also be written as.

$$y(t) = \int_{-\infty}^{\infty} h(\tau)x(t-\tau)d\tau \tag{2}$$

Assuming wide-sense stationarity, the auto-correlation function, can be expressed as

$$R_{yy}(\tau) = \int_{-\infty}^{\infty}\int_{-\infty}^{\infty} R_{xx}(\tau+\rho_1-\rho_2)h(\rho_1)h(\rho_2)d\rho_1 d\rho_2 = R_{xx}(\tau) * h(\tau)h(-\tau) \tag{3}$$

while the cross-correlation functions becomes

$$R_{xy}(\tau) = \int_{-\infty}^{\infty} R_{xx}(\tau-\rho)h(\rho)d\rho = R_{xx}(\tau) * h(\tau) \tag{4}$$

$$R_{yy}(\tau) = \int_{-\infty}^{\infty} R_{xy}(\tau+\rho_1)h(\rho_1)d\rho_1 = R_{xy}(\tau) * h(-\tau) \tag{5}$$

Therefore, by knowing the correlation functions, we also know the impulse response functions of the system. The above could as well have been represented for the frequency domain. For more detail on the above, see [7].

For large structures like bridges, buildings, vessels etc., excitation by means of experimental equipment is not very practical, thus we do not know the input to the system. Therefore, by utilizing Equations 3-5, to extract the frequency response functions from correlation functions, the dynamic properties of the excitation force will be included in the total solution. For wide-sense stationary excitation, this is not an issue. However, the external forces on the structures mentioned in the start of this paragraph, are typically limited to vibrating machinery as well as traffic, wind and wave loads.

When talking MPE, there are two distinct categories, those operating directly in the time domain and those that extend to the frequency domain. Time domain identification extract information from the impulse response function, whilst frequency domain identification reaps information from frequency function.

In the following, the multi-reference Ibrahim Time Domain (MITD) method [8, 9] is used, although the AOMA algorithm, can be implemented for all MPE methods that can produce a stabilization diagram. The MITD method is very similar to the covariance driven SSI. MITD is based on building a Hankel matrix from the correlation functions, which then is solved by means of singular value decomposition in order to extract the states of the system. The size of the Hankel matrix is governed by the model order. It is typical to over-fit the model, thus yielding more poles, but also more spurious poles.

Typically a set of criteria, that governs whether a pole is physical or spurious, are set up. Such criteria can be related to restrictions or expectations to physical properties of the structure. As mentioned in the introduction, the stabilization diagram is a strong tool in separating physical poles from spurious ones.

A popular supplement to the stabilization diagram is the Modal Assurance Criteria given in Equation 6.

$$MAC_{rs} = \frac{\left|\{\psi\}_r^H \{\psi\}_s\right|^2}{\left(\{\psi\}_r^H \{\psi\}_r\right)\left(\{\psi\}_s^H \{\psi\}_s\right)} \tag{6}$$

where ^{H} is the Hermitian transpose (complex conjugate and transpose) and $\{\psi\}r$ and $\{\psi\}s$ are mode shapes originating from modes r and s. The MAC value can take any value between 0 and 1. For independent mode shapes $\{\psi\}_r \neq \{\psi\}_s$ and $MAC_{rs} = 0$, whereas for identical mode shapes $\{\psi\}_r = \{\psi\}_s$ and $MAC_{rs} = 1$.

2.1 Methodology

The proposed methodology is outlined in Figure 1.

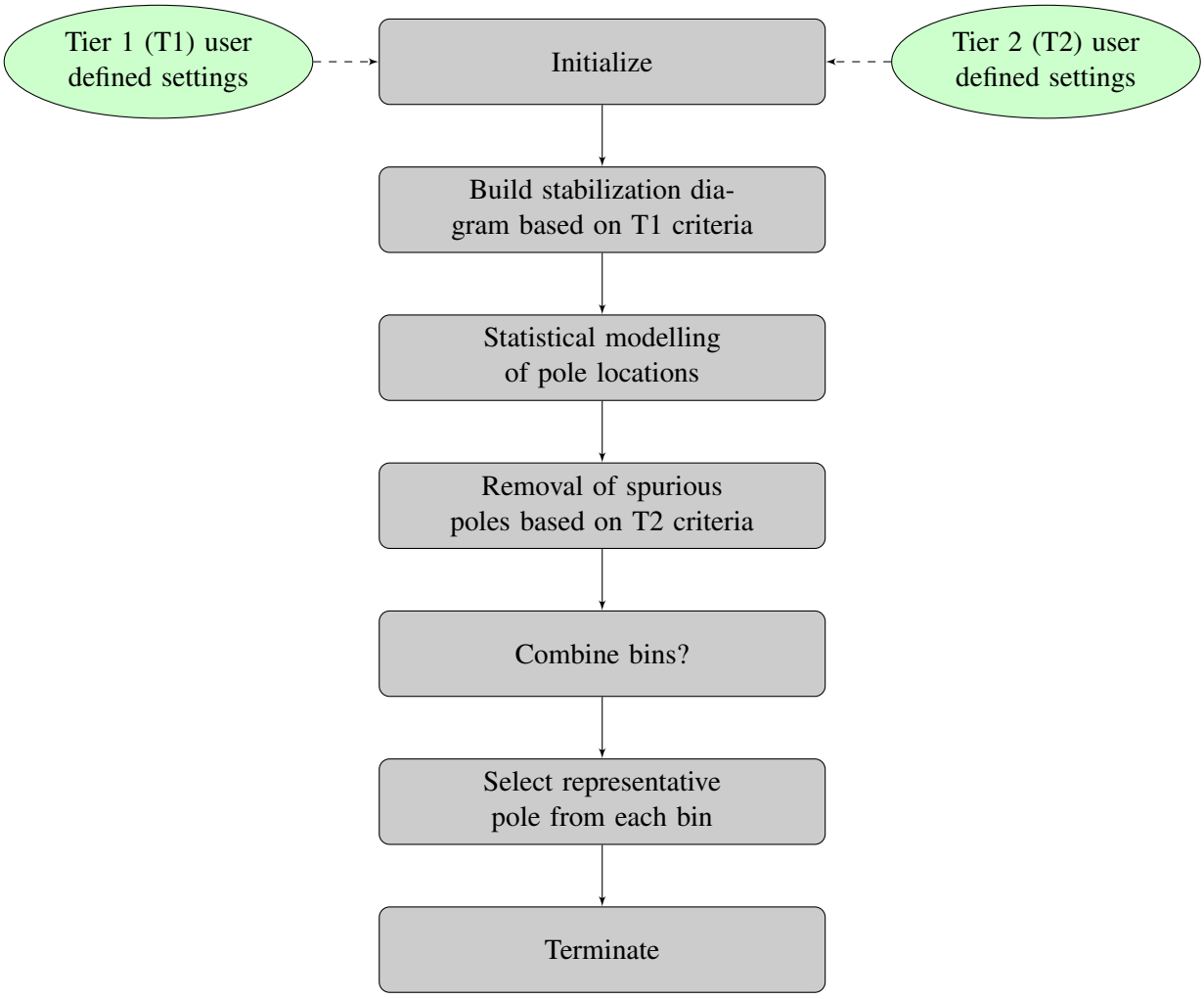

Figure 1: Flowchart of the proposed AOMA algorithm

A set of parameters must be defined before the AOMA algorithm can be initiated. These parameters are presented in Table 1, and are divided into two groups, i.e. Tier 1 and Tier 2. The former Tier is related to the MPE method chosen, which in this case involves assigning a model order and defining how much information that should be used of the correlation function [10, 11]. The latter Tier, on the other hand, is related to the application in question, and involves the statistical parameters that allow for the statistical modelling of the pole locations, and the steps leading to the selection of one representative pole for each mode shape found.

Parameter	Description	Suggested value
Tier 1		
NPoles	Number of poles (model order)	MPE dependent
NStart	First value in IR or CF	MPE dependent
NLines	Number of values in IR or CF	MPE dependent
Tier 2		
minFreq	Minimum frequency	Application dependent
maxFreq	Maximum frequency	Application dependent
NoBins	Number of bins	Application dependent
BinThreshold	Bin size threshold	Application dependent
MACThreshold	MAC value threshold	Application dependent
MinBinSize	Minimum bin size	Application dependent

Table 1: User defined settings

Depending on the application, some *a priori* sorting criteria can be applied to the pole sorting process. For instance, for under-damped systems, all physical poles always come in complex conjugate pairs, or for a suspension bridge, it is unlikely that the damping ratio for the first handful of modes shapes is high.

When the user defined settings are set up, the AOMA algorithm can start, and the stabilization diagram is built based on the Tier 1 user defined settings. A frequency bandwidth is the first parameter in the Tier 2 user defined settings, and dictates the frequency band of interest. The next step is to overlay the stabilization diagram by its probability distribution using the predefined resolution. In the following step, all bins below a certain threshold are discarded from further processing. By intuition, the mode shapes for each bin should have similar characteristics. By utilizing the MAC, a conformity check is made, and poles in each bin, that have poor MAC values in comparison to the majority of the poles in that bin, are removed. The AOMA algorithm is set to use a very high number of bins, and it is therefore possible that adjacent bins have similar MAC properties, if that is the case, they are combined into one bin. The combined bins must pass a check that ensure robustness, i.e. the size of the combined bins must contain a certain number of poles. The last step involves selecting one representative pole for each of the remaining bins. These poles are selected based on Equation 7.

$$\lambda_n = min\left(\left||\bar{\lambda_n}| - |\lambda_{n,i}|\right|\right) \tag{7}$$

where λ_n is the representative pole for bin n, $|\lambda_{n,i}|$ represents the absolute values for the poles in bin n having poles i, while $|\bar{\lambda_n}|$ denotes the average value for the absolute values for the poles in bin n.

3 Results and discussion

Since any measurement is finite, modal parameter estimates will always be erroneous. Good damping estimates require a long measurement duration. The data presented in this paper, can be considered to have sufficiently long measurements times. For more information on the data used, the reader is referred to the articles mentioned in each of the 4 subsections.

The Tier 1 and Tier 2 user defined settings, listed in Table 1, will to some degree have an influence on the estimates of the modal parameters for the proposed methodology for an AOMA algorithm. Variations in the Tier 1 user defined settings do not influence the results much, while altering the Tier 2 user settings has a larger impact. To show the integrity of the AOMA algorithm the same settings, except for the frequency band of interest, are used for all 4 data-sets. This paper is not a parameter study, but rather a demonstration, hence modifications to the Tier 1 and Tier 2 user defined settings will not be investigated further.

For all data-sets, no data were discarded, the correlation functions were produced using a block-size of 512 samples. The model order was chosen to 40 modes (or 80 poles), the first 5 lags were discarded and 100

samples in each correlation function were used. All frequency and damping estimates presented in this section are derived from MITD, that includes results from other papers.

3.1 Plexiglas Plate

The first data-set addresses a laboratory Plexiglas plate measuring 533 x 321 x 20 millimeters, whose response was recorded using 35 out-of-plane oriented uni-axial accelerometers in a double symmetric pattern. All sensors were mounted in the same plane (out-of-plane). The excitation was applied by gently tapping the tip of a pencil randomly around the plate during a measurement period of 5 minutes. This corresponds to approximately 42.500 cycles of the first natural frequency. For more details on the measurements, the reader is referred to [12].

In figure 2, two stabilization diagrams are shown. To the left, the stabilization diagram is overlaid by its probability distribution (step 3 in figure 1). The dashed line represents the bin threshold and the frequency interval of interest $100 - 900Hz$. To the right, MAC stable poles along with the automatically selected representative pole, are shown (step 6 in figure 1).

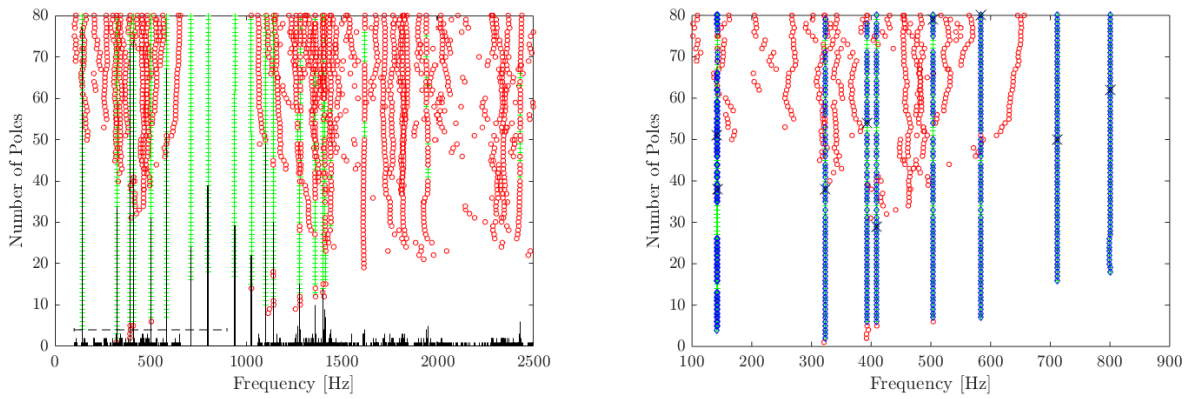

Figure 2: Stabilization diagrams of the modal parameter estimates for the laboratory Plexiglas Plate. Left: Stabilization diagram overlaid by its probability distribution (the dashed line represents the bin threshold and the frequency interval of interest). Right: Stabilization diagram indicating MAC stable poles and the automatically selected representative pole (zoomed into the frequency band of interest). Pole below bin threshold - Red circle ○. Pole above bin threshold - green plus +. Pole that is MAC stable - blue diamond ◇. Representative pole - black cross ×

Looking at the stabilization diagrams, it it clear to see that there is a large number of spurious poles in the frequency band of interest. Many of these spurious poles have one thing in common, being below the bin threshold, while all the remaining poles are above the bin threshold. This tendency accepts the fact that physical poles stabilize on the frequency axis for increasing model order, while spurious poles do not. In the subsequent step of the proposed algorithm the MAC value for each bin is utilized to detect and remove poles, i.e. poles in each bin that have poor MAC value relative to the majority of poles in that bin, are removed. One reason for this, is that it is likely that some spurious poles fall into bins of frequency stable poles. By checking the MAC value, such poles can easily be removed, as seen in the right stabilization diagram in Figure 2. In the final step one representative pole for each bin are picked, and the results are compared to a manual approach.

Automated		Manual	
Frequency, $[Hz]$	Damping, $[\%]$	Frequency, $[Hz]$	Damping, $[\%]$
141.928	3.08	141.904	3.24
142.577	3.10	142.585	3.06
323.177	2.66	323.261	2.67
393.044	2.61	393.045	2.54
408.771	2.52	408.798	2.45
503.724	2.44	503.774	2.41
583.667	2.45	583.571	2.38
712.006	2.41	711.322	2.41
799.829	2.19	798.754	2.27

Table 2: Comparison between the modal parameters found for the laboratory Plexiglas Plate, using the proposed automated procedure, and the manual approach according to [12]

This comparison is shown in Table 2. The AOMA algorithm successfully detects 9 modes, just like the manual approach. The frequency and damping estimates for both approaches are very similar. Furthermore, the AOMA algorithm manages to separate the first two closely spaced modes indicating that they are unique.

3.2 Little Belt Suspension Bridge

The second data-set addresses the Little-belt Suspension Bridge that has a main span of 600 meters, whose response was recorded using 30 horizontally oriented and 15 vertically oriented uni-axial geophones in a double symmetric pattern. All these sensors were mounted and in the same plane inside the closed box girder. The bridge was excited by a combination of wind and traffic loads during a measurement period of 60 minutes. This corresponds to approximately 560 cycles of the first natural frequency. For more details on the measurements, the reader is referred to [13].

In figure 3, two stabilization diagrams are shown. To the left, the stabilization diagram is overlaid by its probability distribution (step 3 in figure 1). The dashed line represents the bin threshold and the frequency interval of interest $0.05 - 0.9Hz$. To the right, MAC stable poles along with the automatically selected representative pole, are shown (step 6 in figure 1).

For these stabilization diagrams the frequency band of interest consists primarily of frequency stable poles, while at higher frequencies ($> 1.5Hz$), the stabilization diagrams are highly contaminated by spurious poles. The high number of spurious poles are related to the sampling frequency and the model order. For increasing model order, the number of poles (twice the model order), must be squeezed into a frequency interval, that is limited by a lower bound, DC ($0Hz$) and a higher bound, $f_s/2$, where f_s is the sampling frequency. The sampling frequency can be adjusted by down-sampling the original signal to an appropriate level. The model order must be selected accordingly. A compromise between choosing the right combination of model order and the sampling frequency is therefore necessary, for two reasons, to ensure that enough frequency stable poles are available, but also to keep the number of spurious poles to a minimum. In the stabilization diagram to the right in Figure 3, only a few poles were removed due to having poor MAC values relative to the majority of poles in their respective bin. The poles removed are concentrated around a model order of 18 (36 poles).

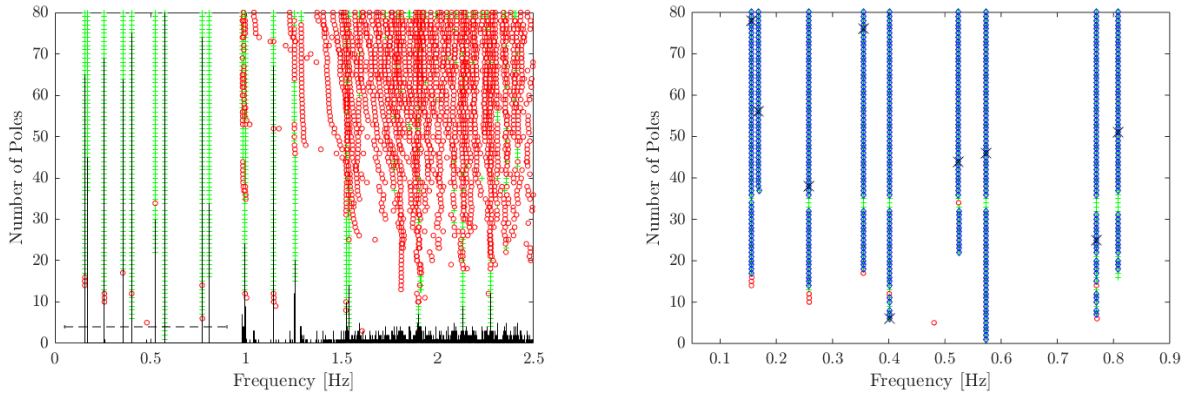

Figure 3: Stabilization diagrams of the modal parameter estimates for the Little Belt Suspension Bridge. Left: Stabilization diagram overlaid by its probability distribution (the dashed line represents the bin threshold and the frequency interval of interest). Right: Stabilization diagram indicating MAC stable poles and the automatically selected representative pole (zoomed into the frequency band of interest). Pole below bin threshold - Red circle ○. Pole above bin threshold - green plus +. Pole that is MAC stable - blue diamond ◇. Representative pole - black cross ×

Automated		**Manual**	
Frequency, $[Hz]$	Damping, $[\%]$	Frequency, $[Hz]$	Damping, $[\%]$
0.156	1.91	0.156	3.15
0.169	12.01	0.171	9.74
0.258	0.83	0.258	0.78
0.355	1.64	0.355	1.77
0.401	0.99	0.401	0.93
0.524	0.72	0.523	0.76
0.573	0.40	0.573	0.38
0.769	0.58	0.769	0.60
0.808	0.56	0.808	0.69

Table 3: Comparison between the modal parameters found for the Little Belt Suspension Bridge, using the proposed automated procedure, and the manual approach according to [13]

The AOMA algorithm successfully finds a total of 9 modes, which was also the case when using a manual approach, see [13]. The frequency estimates reported by the two approaches show resemblance. For the damping estimates found for the first two modes, the reported values using the AOMA algorithm are more distant from one another, in comparison to the damping estimates reported using the manual approach. In [13] it was found that by adjusting the number of lags used in the correlation function, the damping estimates for these two modes varied significantly. No particular pattern was detected, but a likely cause for this behavior is thought to be related to a close coupling of two modes, one mode with low damping and one mode with high damping. For the remaining 7 modes the damping estimates, for the two approaches, are within the boundary of acceptance.

3.3 Heritage Court Tower

The third data-set addresses the Heritage Court Tower located in downtown Vancouver, British Columbia in Canada. It is a medium-rise building measuring approximately 42.5 meters in height. The typical floor dimension is 25 x 31 meters, while the 3 lower levels measure 36 x 30 meters. The response was recorded

using 5 northerly oriented and 3 westerly oriented uni-axial accelerometers. The sensors were installed on the northern facade at 3 different levels. In the full study of the building, more sensors were available, but in this paper, only the data from setup 4 are used. The medium-rise building was primarily excited by wind loads during a measurement period of 10 minutes. This corresponds to approximately 725 cycles of the first natural frequency. For more details on the measurements, the reader is referred to [14].

In figure 4, two stabilization diagrams are shown. To the left, the stabilization diagram is overlaid by its probability distribution (step 3 in figure 1). The dashed line represents the bin threshold and the frequency interval of interest, $0.5 - 1.75Hz$. To the right, MAC stable poles along with the automatically selected representative pole, are shown (step 6 in figure 1).

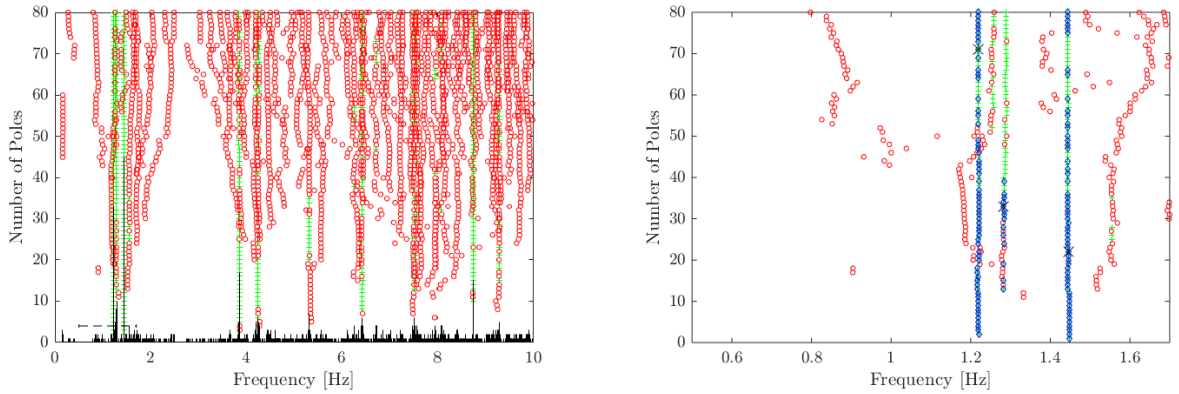

Figure 4: Stabilization diagrams of the modal parameter estimates for the Heritage Court Tower. Left: Stabilization diagram overlaid by its probability distribution (the dashed line represents the bin threshold and the frequency interval of interest). Right: Stabilization diagram indicating MAC stable poles and the automatically selected representative pole (zoomed into the frequency band of interest). Pole below bin threshold - Red circle ○. Pole above bin threshold - green plus +. Pole that is MAC stable - blue diamond ◇. Representative pole - black cross ×

In these stabilization diagrams, there are many spurious poles, both in the frequency band of interest and on either side of it. The AOMA algorithm manages the initial removal of spurious poles and the subsequent deselection of poles with poor MAC values. Finally one representative pole for each of the 3 modes within the frequency band of interest are selected. On the right-hand side stabilization diagram in Figure 4, it can be seen that there are many representative poles for the first and third mode, while for the second mode the number of representative poles are scarce. It is likely that this mode is weakly excited. However, the AOMA algorithm is still able to overcome this challenge.

Automated		**Manual**	
Frequency, $[Hz]$	Damping, $[\%]$	Frequency, $[Hz]$	Damping, $[\%]$
1.220	1.66	1.245	1.05
1.283	1.46	1.299	1.40
1.445	1.16	1.441	0.31

Table 4: Comparison between the modal parameters found for the Heritage Court Tower, using the proposed automated procedure, and the manual approach according to [14]

When comparing the results for the two procedures, namely the AOMA algorithm and the manual approach in [14], it is evident that the frequency estimates are agreeing well. However, for the damping estimates there are some discrepancies, especially for the third mode, which for the manual approach is reported at 0.31%,

whilst for the proposed AOMA algorithm it is 1.16%. The representative pole is selected based on Equation 7. For the 57 poles, the damping estimate is within 1.13% - 1.51%.

3.4 Ro-Lo Ship

The fourth data-set addresses a roll-on lift-off (Ro-Lo) ship with a total length of 210 meters and a width at main deck of 29.6 meters. The response was recorded using 22 horizontally oriented and 11 vertically oriented uni-axial accelerometers in a double symmetric pattern. All these sensors were mounted in the same plane at the main deck of the ship. Furthermore, the bow and stern were represented by 2 measurement points, each (2x2) measuring in all 3 directions (x,y,z). The ship was traveling at 18 knots in a calm sea state, hence it was primarily excited by the propeller loads as well as relative wave and wind loads during a measurement period of 90 minutes. This corresponds to approximately 4700 cycles of the first natural frequency. For more details on the measurements, the reader is referred to [15].

In figure 5, two stabilization diagrams are shown. To the left, the stabilization diagram is overlaid by its probability distribution (step 3 in figure 1). The dashed line represents the bin threshold and the frequency interval of interest, $0.5 - 4.0Hz$. To the right, MAC stable poles along with the automatically selected representative pole, are shown (step 6 in figure 1).

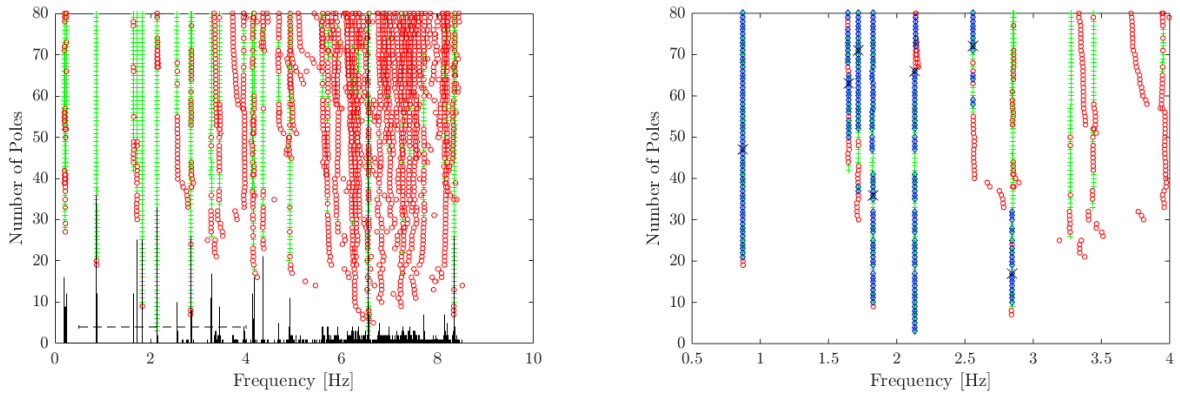

Figure 5: Stabilization diagrams of the modal parameter estimates for the Ro-Lo Ship. Left: Stabilization diagram overlaid by its probability distribution (the dashed line represents the bin threshold and the frequency interval of interest). Right: Stabilization diagram indicating MAC stable poles and the automatically selected representative pole (zoomed into the frequency band of interest). Pole below bin threshold - Red circle $\circ$. Pole above bin threshold - green plus $+$. Pole that is MAC stable - blue diamond $\diamond$. Representative pole - black cross $\times$

For the stabilization diagrams shown in Figure 5 the same tendency as for the Little Belt Suspension bridge is present, i.e. a large number of spurious poles are located at the higher frequencies ($> 5Hz\%$), also see Figure 3. In the frequency interval of interest there are a large sum of spurious poles. These are easily identified. Looking at the frequency interval in more detail, the first 5 modes are well represented by a sufficient number of poles. The 6th and 7th mode are represented, but with fewer poles. The automated algorithm cannot detect any modes between $3 - 4Hz$, though the experienced eye, can see an indication of up to 3 additional modes. The first column of poles appear to be frequency stable, but does not pass the MAC check, that ensures that only poles sharing the same MAC properties can qualify for any subsequent steps. This algorithm is looking for well represented mode shapes, and is not intended for separating mode shapes due to weakly excited modes, faulty equipment, missing sensors etc.

Automated		Manual	
Frequency, $[Hz]$	Damping, $[\%]$	Frequency, $[Hz]$	Damping, $[\%]$
0.871	1.78	0.871	1.62
1.647	0.27	N/A	N/A
1.718	1.09	1.723	1.36
1.825	0.88	1.823	0.94
2.135	1.13	2.137	1.07
2.558	1.60	2.538	1.09
2.846	0.93	2.856	1.62
N/A	N/A	3.273	0.14
N/A	N/A	3.425	1.73
N/A	N/A	3.956	1.92

Table 5: Comparison between the modal parameters found for the Ro-Lo Ship, using the proposed automated procedure, and the manual approach according to [15]

The AOMA algorithm detected 7 modes in the data-set, 6 of these modes were also reported by the manual approach, see Table 5. The manual approach were also able to detect the 3 higher order modes at $3.273Hz$, $3.425Hz$ and $3.956Hz$. The mode found at $1.647Hz$ is a harmonic and is also present in [15]. This algorithm is not designed to remove harmonics, but confirms that harmonics can be both frequency stable, and have similar MAC characteristics. For harmonic removal the reader is referred to [16]. Comparing the modes that were actually found, it is evident that the frequency estimates for the two procedures are similar. The damping estimates for the first 4 modes are complementing each other well, while for the last two modes, at $2.558Hz$ and $2.846Hz$, there are some discrepancies. The number of representative poles at these two modes are few. A possible explanation for the noticeable deviation in damping estimates could be that since a large number of non-representative poles was removed by the AOMA algorithm, a manual approach could just as well have selected one of such poles.

4 Conclusion

The proposed AOMA algorithm faced a number of challenges, in particular, closely spaced modes, weakly excited modes and harmonics. It could not distinguish harmonics from non-harmonic modes, but have overall shown to successfully identify well represented modes in an automated way, by using a combination of statistic moddeling of the pole locations, and a decision rule based on the MAC value of individual poles.

Acknowledgements

The work presented is supported by the INTERREG 5A Germany-Denmark program, with funding from the European Fund for Regional Development. Also a thanks to the great people involved in collecting and their willingness to share the data processed in this paper. This is a huge opportunity to develop tools that work on different applications in a robust way.

References

[1] R. J. Allemang, D. L. Brown, *A Unified Matrix Polynomial Approach to Model Identification*, Journal of Sound and Vibration, Vol. 211, No. 3, pp. 301-322.

[2] G. Zhang, J. Mab, Z. Chen, R. Wang, *Automated Eigensystem Realisation Algorithm for Operational Modal Analysis*, Journal of Sound and Vibration, Vol. 333, 2014, pp. 35503563.

[3] C. Devriendt, F. Magalhes, W. Weijtjens, G. De Sitter, . Cunha, P. Guillaume, *Structural Health Monitoring of Offshore Wind Turbines using Automated Operational Modal Analysis*, Structural Health Monitoring, Vol. 13(6), 2014, pp. 644659.

[4] R. Cardoso, A. Cury, F. Barbosa, *A Robust Methodology for Modal Parameters Estimation Applied to SHM*, Mechanical Systems and Signal Processing, Vol. 95, 2017, pp. 2441.

[5] E. Neu, F. Janser, A. A. Khatibi, A. C. Orifici, *Fully Automated Operational Modal Analysis using multi-stage clustering*, Mechanical Systems and Signal Processing, Vol.84, 2017, pp. 308323.

[6] M. Scionti, J. Lanslots, I. Goethals, A. Vecchio, H. Van der Auweraer, B. Peeters, B. De Moor, *Tools To Improve Detection of Structural Changes From In-Flight Flutter Data*, Proceedings of The 8th International Conference on Recent Advances in Structural Dynamics(IVSR), Southampton, UK, 2004 July.

[7] W. C. van Etten, *Introduction to Random Signals and Noise*, John Wiley & Sons, University of Twente, The Netherlands, 2005.

[8] S. R. Ibrahim, E. C. Mikulcik, *A Method for the Direct Identification of Vibration Parameters from the Free Response*, Shock and Vibration Bulletin, Vol. 47, 1977, pp. 183-198.

[9] K. Fukuzono, *Investigation of Multiple Reference Ibrahim Time Domain Modal Parameter Estimation Technique*, M.S. Thesis, Dept. of Mechanical and Industry Engineering, University of Cincinnati, 1986.

[10] M. Tarpo, P. Olsen, S. Amador, M. Juul, R. Brincker, *On Minimizing the Influence of the Noise Tail of Correlation Functions in Operational Modal Analysis*, Procedia Engineering, Vol. 199, 2017, pp. 1038-1043.

[11] E. Orlowitz, A. Brandt, S. Amador, M. Juul, R. Brincker, *Influence of Noise in Correlation Function Estimates for Operational Modal Analysis*, XXXVI International Modal Analysis Conference, 2018.

[12] E. Orlowitz, A. Brandt, *Comparison of Experimental and Operational Modal Analysis on a Laboratory Test Plate*, Measurement, Vol. 102, 2017, pp. 121-130.

[13] S. S. Christensen, M. S. Andersen, A. Brandt, *Dynamic Characterization of the Little Belt Suspension Bridge by Operational Modal Analysis*, Dynamics of Civil Structures, Vol. 2, 2017.

[14] R. Brincker, C. E. Ventura, *Introduction to Operational Modal Analysis*, John Wiley & Sons, Technical University of Denmark, Denmark, 2015.

[15] E. Orlowitz, A. Brandt, *Operational Modal Analysis for Dynamic Characterization of a Ro-Lo Ship*, Journal of Ship Research, Vol. 58, No. 4, December 2014, pp. 216-224.

[16] A. Brandt, *Comparison and Assessment of Methods to Treat Harmonics in Operational Modal Analysis*, International Conference on Structural Engineering Dynamics, Lagos, Portugal, 2015 June.